




On flapping jets induced by a fluttering film and from circular nozzles of smooth contraction, orifice plate and long pipe

Mengwei Wu¹ · Chunwei Li² · Chuanqing Zhu² · Guochang Wang² · Minyi Xu² · Jianchun Mi^{1,2} 

Received: 11 August 2021 / Revised: 20 February 2022 / Accepted: 1 April 2022
© The Author(s), under exclusive licence to Springer-Verlag GmbH Germany, part of Springer Nature 2022

Abstract

A novel method for the self-excitation of a flapping jet by a flexible film has been developed recently by Xu et al. (*Exp. Ther. Fluid Sci.* 2019, 106, 226–233). The present work is to advance our understanding of this kind of oscillating jets by experimentally examine their dependence on initial flow condition. Specifically, detailed investigations are made on characteristics of both film flutter and jet mixing due to initially distinct flow conditions made by circular nozzles of smooth contraction (SC), orifice plate (OP) and long pipe (LP). Present flapping jets are self-excited by a rectangular FEP film with one end fixed at the nozzle exit. Hot wire anemometry and laser-sheet flow visualization are adopted for the present experiments. Experimental results demonstrate that the film-flutter characteristics are considerably nozzle-dependent. In particular, the OP nozzle yields the largest film-flutter domain and the lowest energy loss for fluttering. It is also shown that the three nozzles' flapping jets exhibit substantially different mixing characteristics due to their distinct initial conditions. Specifically, the OP jet exhibits the highest flapping Strouhal number, highest velocity decay rate, strongest relative turbulence intensity, and largest length scales of turbulence. And the flapping SC and LP jets are compatible in mixing characteristics. Relative to the conventional (non-flapping) free jets, all the present flapping jets entrain and mix the surrounding fluid at a much higher rate, consequently spreading and decaying far more rapidly. Importantly, when the flapping Strouhal number is sufficiently high or low, the small-scale mixing appears to be enhanced or depressed by the flapping in the near field and then maintain farther downstream.

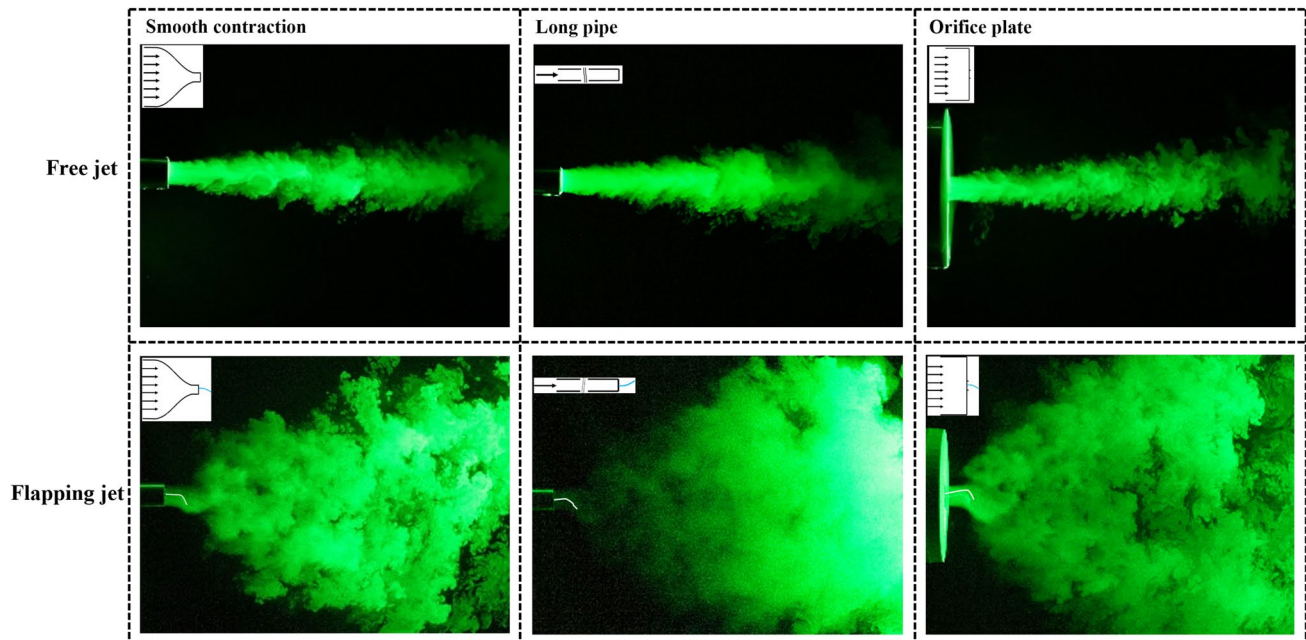
✉ Minyi Xu
xuminyi@dlnu.edu.cn

✉ Jianchun Mi
jmi@pku.edu.cn

¹ College of Engineering, Peking University, Beijing 100871, China

² Marine Engineering College, Dalian Maritime University, Dalian 116026, China

Graphical abstract



1 Introduction

Turbulent jets play an important role, as a method of mixing different fluids, in many applications such as burners and chemical reactors. Therefore, the control of jet mixing, actively with external power supply or passively without external energy supply, has always been a very dynamic research area. To enhance jet mixing, a large body of experimental work (e.g., Crow and Champagne 1971; Hill and Greene 1977; Simmons et al. 1981; Favre-Marinet et al. 1981; Davis 1982; Parekh et al. 1983; Raman and Cornelius 1995; Glauser and Walker 1988) was conducted on jet control during 1970–1990; see Reynolds et al. (2003) for more relevant references. There are many common forms of active controls, e.g., acoustic excitation (Crow and Champagne 1971; Hill and Greene 1977; Parekh et al. 1983) and mechanical excitation involving moving parts (Simmons et al. 1981; Davis 1982). The acoustic excitation of the jet is usually achieved through the loudspeaker in the nozzle, using the natural coupling of flow instability and acoustic resonance to increase the coherence and intensity of large-scale motion (Hill and Greene 1977). Another way to enhance jet mixing is to use a mechanically oscillating nozzle (e.g., Simmons et al. 1981). Furthermore, the active control of jet mixing is also studied successfully by numerical simulations (e.g., Danaïla and Boersma 2000; Gohil et al.

2015; Silva and Métais 2002; Tyliczszak and Geurts 2014; Tyliczszak 2015).

These active excitation technologies are quite effective in laboratory studies but are infeasible and ineffective in practical applications due to their weight, power, and maintenance requirements. For practical applications, the excitation techniques need to be free, without mechanically moving parts, but effective. In this context, passive methods are more feasible. Several practical self-excited nozzles were developed to enhance jet mixing, e.g., the flip-flop jets (Viets 1975; Mi et al. 2001a, b, c), precession jets (Nathan et al. 1998) and oscillating jets (Mi et al. 2004). These “passive control” devices naturally excite the jet itself into oscillation over time. Such a global oscillation is aerodynamically self-excited, and so its generators are named ‘fluidic’ devices, which have important applications in various process industries. In addition, it is also worthy to investigate the jet flows controlled with fluidic devices as they involve numerous fundamental flow features (e.g., Nathan and Luxton 1991; Manias and Nathan 1993).

However, the above fluidic method is not flexible and cannot adapt itself according to the actual situation during operation. Recently, Xu et al. (2019) developed a new type of ‘self-excited’ oscillating jets whose flapping motion is induced by a flexible film with one end fixed at a nozzle exit. Compared with the traditional fluidic methods, this film-flutter jet can adapt to different working conditions easily

by changing the size, shape, and position of the film to optimize the mixing performance. Moreover, the film-flutter jet is expected to have a much smaller pressure loss than the fluidic nozzles. Very recently, Wu et al. (2020) further investigated by experiment the mixing characteristics of the film-flutter jet. Their work suggested that the jet-flapping motion may enhance the turbulence intensity at both large and small fluctuation scales. This, if true, would be inconsistent with Mi et al. (2001a) who claimed that “the dynamic flapping motion enhances the large-scale mixing of the jet while concurrently suppressing the generation of the fine-scale turbulence”.

The above jet-flapping motion is induced by the flutter of a flexible film with one end fixed at a nozzle exit. That is, our previous studies (Xu et al. 2019; Wu et al. 2020) were both associated with the typical problem of fluid–structure interaction, i.e., film flutter. In the past, the flutter of a cantilevered flexible plate (e.g., paper, wooden plate, metal sheet, and plastic film) was extensively investigated in a uniform flow made by low-turbulence wind tunnel (e.g., Païdoussis 2016; Taneda 1968; Eloy et al. 2012). Xu et al. (2019) successfully examined the film flutter characteristics at the exit of a smooth contraction (SC) nozzle, which produces nearly uniform mean velocity distribution and low turbulence intensity. Note that actual fluid jets issue usually from three different types of geometric configuration of jet nozzles, i.e., smooth contraction (SC), long pipe (LP), and orifice plate (OP) (Mi et al. 2001b and 2001c). The SC nozzle generates a uniform “top-hat” velocity profile and laminar flow at the nozzle exit (Mi et al. 2001b). The LP jet is initially in a fully turbulent state from the pipe exit, where the mean velocity usually takes a power-law profile with high turbulence intensity (Mi et al. 2001b). In contrast, the OP jet has a *M*-shaped exit velocity profile and complex vena-contracta flow very near to the nozzle (Mi et al. 2001c). If a film is attached respectively to these nozzles, the resulting flutter characteristics are expected to be distinct, while the corresponding flapping jets would exhibit different mixing characteristics. This is deduced from the work of Mi et al. (2001c), who directly compared the scalar fields of the SC, LP and OP free jets and confirmed that the mixing fields of the three jets are fairly different. In particular, the OP jet was found to behave very differently from the other two jets, e.g., entraining the ambient fluid at the highest rate.

Following the above comments, the present work is designated to investigate the effects of different nozzle-exit flow conditions on the film flutter and turbulent mixing characteristics of a flapping jet. Specifically, the main objective is twofold: i.e.,

- (1) To characterize the film flutter and the jet-flapping frequency when using the SC, LP and OP nozzles.
- (2) To investigate and compare the turbulent mixing characteristics of the flapping jets from the three nozzles versus their non-flapping counterparts.

The rest of the paper is presented as follows. Section 2 shows experimental details including the setup and test conditions. In Sect. 3, we analyze and discuss the experimental results. At last, several concluding remarks are made in Sect. 4.

2 Experimental details

2.1 Facility setup

Figure 1 displays the present experimental facilities, including schematics of a smooth contraction (SC), an orifice plate (OP), and a long pipe (LP) nozzles of the exit diameter $D = 40$ mm, together with a film attached at its leading edge. A LabVIEW-based computer is used to control the frequency converter, and further to control the voltage of the blower to generate a desired flow rate and speed. The blower outlet is connected to a 1.5 m long rectifier box equipped with a honeycomb and a metal mesh to improve the flow conditions, thereby improving data quality. The (x, y, z) coordinate origin is selected at the center of the nozzle outlet, where x is the downstream distance measured from the nozzle exit, and y is the transverse distance from the centerline and perpendicular to the span or width of the film. The choice of this coordinate system allows the flapping and non-flapping (free) jets to have the same initial conditions. It is worth noting that the film flaps primarily in the y direction. The hot-wire measurement range is $x/D = 0–21$. The mixing characteristics of the film-flutter flapping jet versus the free-from-film non-flapping jet (simply named “free jet” below) are studied at the exit Reynolds number of $Re = 30,000$, where $Re \equiv U_0 D / \nu$, with U_0 and ν being the jet-exit velocity and fluid kinematic viscosity, respectively.

We use rectangular films of FEP (fluorinated ethylene propylene) with a thickness of 50 μm . Each film is fixed to the nozzle exit using a small clip with the thickness of 1 mm made through a 3D printer. In order to ensure the balance of the force on both film sides, two pieces of the same clip are used to fix the film in the nozzle middle. Attention has been paid to minimize the influence of clips by carefully selecting each clip. If the clip is too big, vortices may be generated, which will affect the film flutter. Moreover, to measure the pressure loss due to the film flutter, a differential pressure gage is used and located upstream of the nozzle exit as shown in Fig. 1.

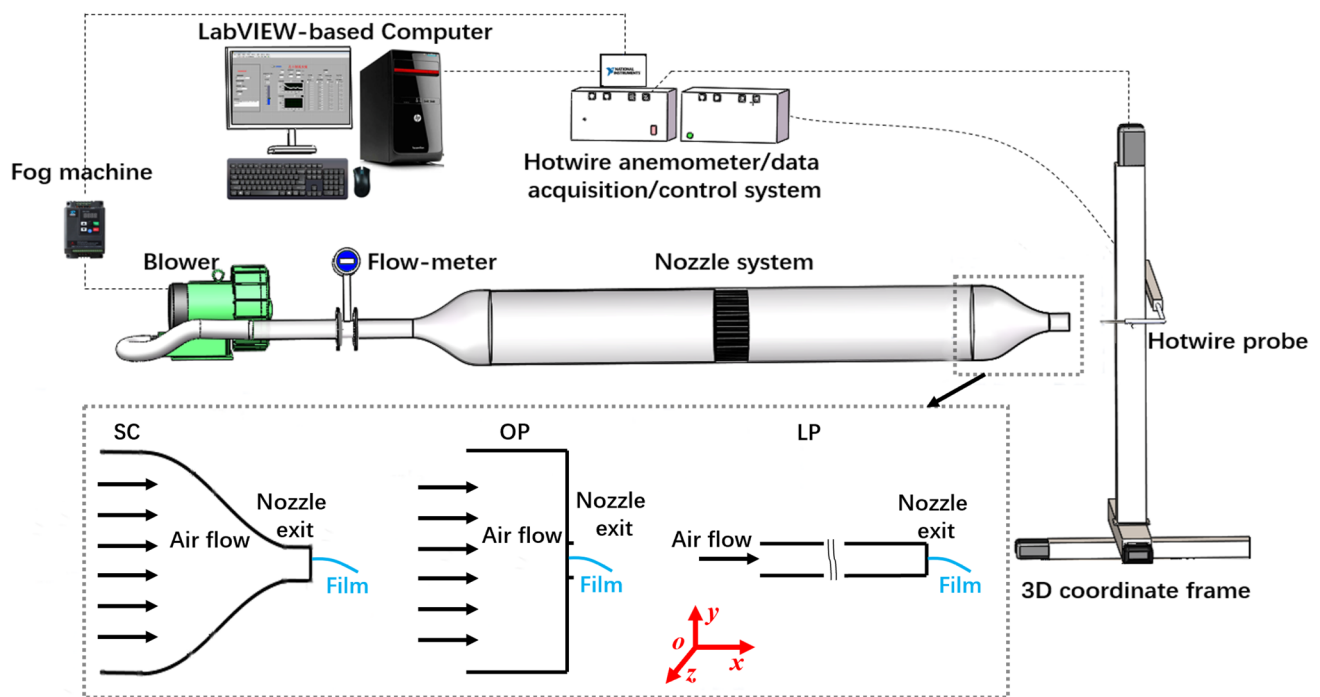


Fig. 1 Experimental facilities and schematics of a smooth contraction (SC), orifice plate (OP), long pipe (LP) nozzles with a film and the definition of the coordinate system

2.2 Flow visualization

To investigate the instantaneous flow characteristics of film fluttering, flow visualizations are conducted using smoke illuminated by a class IV laser (wavelength is 532 nm with peak power less than 10 W). The laser sheet is parallel to the xy plane and the illuminated area extends to about 1000 mm in the x -direction and about 500 mm in the y -direction. Images are taken using a Canon camera (EOS 5D Mark iii) with the focal length of 24~105 mm. The smoking is realized by a fog machine, with the spray volume of 11.8 m³/s and nozzle diameter of 1.0 mm. The mixing of the working fluid and seeding fog occurs in a reservoir located upstream of the stagnation chamber.

2.3 Hot-wire anemometry

To determine the flapping frequency f_F and examine the flapping-jet velocity field, a single hot-wire probe is used to measure the streamwise velocity (U); note that the probe is positioned through a three-dimensional coordinate control system, as shown in Fig. 1. The tungsten hot-wire of 5 μ m in diameter and approximately 1 mm in active length is operated by an in-house constant temperature circuit at an overheat ratio of 1.5. The signals through the circuit are offset, amplified and then digitized by a personal computer with a 12-bit A/D converter at a sampling frequency of 50 kHz for

120 s. The hot-wire is calibrated against a miniature standard pitot tube in the low-turbulence ($\approx 0.6\%$) unmixed core of the jet from the smoothly contracting circular nozzle. Calibrations are performed before and after each set of measurements. Third order polynomial curves are used to fit the calibration data, i.e., $U = a_0 + a_1E + a_2E^2 + a_3E^3$ where E is the voltage over the hot-wire at a given velocity U measured by the pitot tube and a_i ($i = 1 \sim 3$) are the calibration constants.

3 Results and discussion

3.1 Initial mean and RMS velocity profiles

Figure 2a, b shows the normalized nozzle-exit mean and RMS velocity (U_e/U_{ec} and u_e'/U_{ec}) profiles obtained at $x/D = 0.1$ in the SC, LP and OP jets for $Re = 30,000$. Here, U_e and U_{ec} are the exit mean velocity and its centerline value, respectively, while the RMS $u_e' = \langle u_e'^2 \rangle^{1/2}$. Figure 2a indicates distinct differences in the exit profiles of both U_e/U_{ec} and u_e'/U_{ec} between the three jets. The distributions of U_e/U_{ec} for the three jets are similar to those of Mi et al. (2001c). More specifically, the mean profile is shaped like a ‘top-hat’ for the SC nozzle while that for the LP jet is well described by the one-fifth power law which relates to a fully-developed pipe flow. Highly notably, the profile for the OP jet differs greatly from those of the SC and LP jets, with

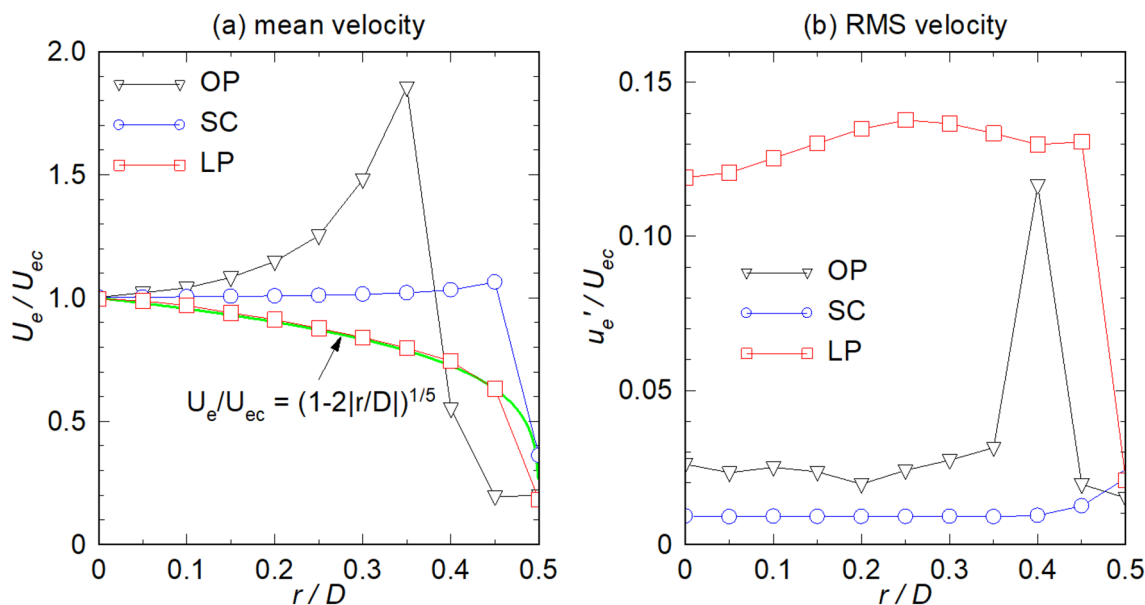


Fig. 2 Radial normalized profiles of the exit mean (U_e) and RMS (u'_e) velocities obtained at $x/D=0.1$ in the jets issuing from the SC, LP and OP nozzles: **a** U_e/U_{ec} and **b** u'_e/U_{ec}

the maximum velocity being almost 1.9 times of the center-line value and locating at $r/D \approx 0.35$. Similarly, significant distinctions occur in the initial profiles of u'_e/U_{ec} between the three jets. For the SC nozzle, the relative turbulence intensity is about 0.9% at $r < 0.45D$ and ~3% in the thin shear layer at $r > 0.45D$. For the OP nozzle, the turbulence is relatively higher, with $u'_e/U_{ec} \approx 2.5\%$ at $r/D \leq 0.35$ and 12% at $r/D \approx 0.4$. In contrast, for the LP nozzle, the relative turbulence intensity is generally much higher at $u'_e/U_{ec} > 10\%$ throughout the exit plane. Above all, the velocity profiles shown in Fig. 2a, b can be considered as the initial flow conditions of the three jets that may influence the jet mixing and film flutter characteristics.

3.2 Film flutter characteristics with different nozzles

3.2.1 Pressure loss due to the film and its flutter

The film flutter at the nozzle exit is expected to cause some pressure loss versus the non-film case or the free jet. We measured the loss for varying the film length at $L/D=0-2.0$ in the jets at $Re=30,000$ using a differential pressure gage as seen in Fig. 1. The results are shown in Table 1. For $L/D=0$ (free jet), the pressure losses caused only by the SC, LP and OP nozzles themselves without film are 100.4, 32.4 and 185 Pa. These pressure losses grow when attaching a film to each nozzle exit and fluttering. On average, the loss growths are about 3.5, 2.9 and 1.6 Pa, respectively, for the SC, LP and OP nozzles. These small numbers indicate low energy losses from the film flutter, which are approximately 3.5% (SC), 10.4% (LP) and 0.8% (OP) of the pressure losses due

Table 1 Pressure loss (Pa) under three nozzle conditions

L/D	SC (Pa)	ΔP_{SC}	$C_{p_{SC}}$	LP (Pa)	ΔP_{LP}	$C_{p_{LP}}$	OP (Pa)	ΔP_{OP}	$C_{p_{OP}}$
0	100.4	0	0	32.4	0	0	185	0	0
0.5	103.9	3.5	0.52	32.6	0.2	0.03	186.3	1.3	0.19
0.75	105.3	4.9	0.72	34.8	2.4	0.35	187.2	2.2	0.32
1.0	103.9	3.5	0.52	35.5	3.1	0.46	186.0	1.0	0.15
1.25	102.8	2.4	0.35	37.5	5.1	0.75	186.4	1.4	0.21
1.5	103.7	3.3	0.49	35.7	3.3	0.49	186.7	1.7	0.25
2.0	103.7	3.3	0.49	35.6	3.2	0.47	186.7	1.7	0.25
mean($L/D > 0$)	103.88	3.48	0.51	35.28	2.89	0.43	186.55	1.55	0.23

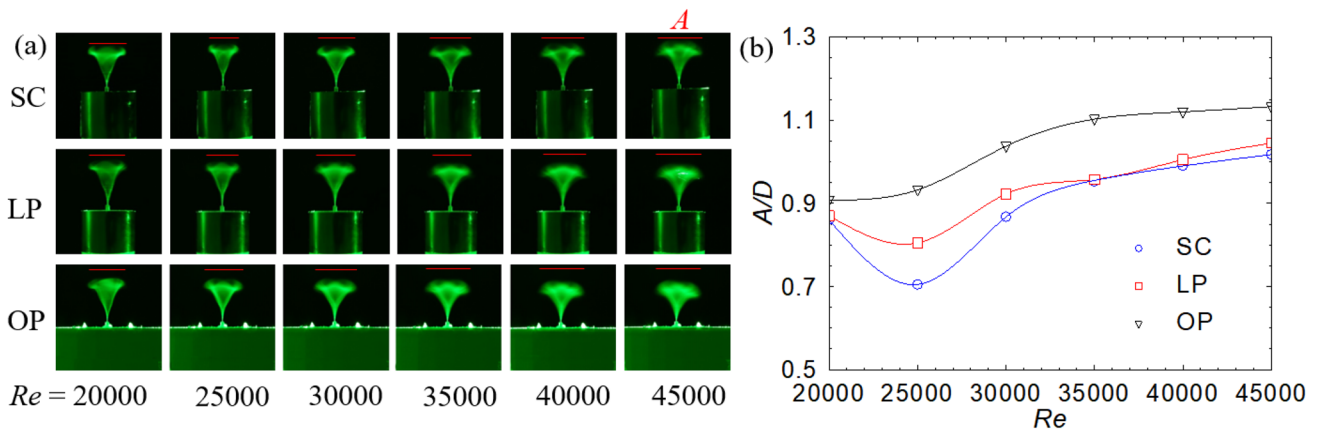


Fig. 3 **a** Long-exposure (20 s) photographs of a fluttering film and **b** normalized maximal amplitude (A/D) of film flutter versus Reynolds number (Re) for three nozzle cases

to the jet nozzles themselves. In particular, the least loss of the film flutter occurs from the orifice nozzle.

3.2.2 Film flutter amplitude and domain

Figure 3a shows the photos of 20 s exposure for fluttering of a film with $L = 1.0D$ fixed at the three nozzle exits. These images were taken for six different Reynolds numbers ($Re = 20,000$ – $45,000$). The maximum of the flutter amplitude (A) for each case is indicated by a red line on the related image in Fig. 3a. To examine the A - Re relationship, Fig. 3b illustrates the normalized result of A/D versus Re . Apparently, as Re rises from 20,000, the amplitude (A) reduces first and then increases for the SC and LP cases while A increases all the way for the OP case. It is also observed in Fig. 3 that the OP film flutters at a significantly greater amplitude than do the SC and LP films. The previous work, e.g., Mi et al. (2001c), revealed that, distinct from the other two jets, the OP jet exhibits a vena contracta immediately downstream from the exit plane, which causes the OP jet to flap more easily and also more widely. Hence, it is deduced that the film can flutter in a greater amplitude in the OP jet than in other two jets.

Figure 4 shows the critical Reynolds numbers (Re_{cf} & Re_{cr}) against L/D for the flutter domain of an FEP film. Here, Re_{cf} is the minimum Reynolds number at which the film onsets to flutter as the jet exit speed (U_o) rises, while Re_{cr} is that for the film to start resting as U_o drops. Figure 4 demonstrates that Re_{cr} is always smaller than Re_{cf} no matter how L is changed and which nozzle is used. This phenomenon is normally called hysteresis, and was considered by Eloy et al. (2012) to result initially from an inherent flatness defect in the plate or membrane. However, Xu et al. (2019) took this naturally as an inertial phenomenon: whether the film planarity is perfect or not, a film always starts fluttering at a higher U_o than that for the film to rest. Moreover, it is

observed that as L increases, both Re_{cf} and Re_{cr} for all the nozzles decrease significantly. The reason for this observation is that any longer film is easier to flutter than the shorter one, due to weakening the bending stiffness.

Figure 4d compares the film-flutter domains, or the variations of Re_{cf} versus L/D , for the three nozzle cases. It is quite evident that, overall, the flutter domain is largest for the OP film and smallest for the LP film. More specifically, for $L/D = 0.5 \sim 1.7$, the film flutter onsets at lower Re_{cf} or initial jet speed for the OP than LP and SC nozzles.

3.3 Jet-flapping frequency and Strouhal number

While the flutter of a flexible film can be seen directly by our eyes, Fig. 3a, an air jet and its flapping motion (if any) cannot. However, they can be visualized indirectly by smoking the jet flow. Figure 5 shows typical instantaneous images of the smoked jets at $Re = 30,000$ without (Fig. 5(a1–c1), (a3–c3)) and with (Fig. 5(a2–c2), (a4–c4)) a film being attached to each nozzle. It is obvious that a fluttering film induces the jet to flap and then to make the jet spreading laterally at a much larger angle than does a free jet. Nevertheless, Fig. 5 provides only a rough and overall appearance but no detailed information about the flapping jets, from which only visual or qualitative observations can be made. So, we need to examine below the flapping frequency and its dimensionless value—Strouhal number.

The previous experiments (e.g., Païdoussis 2016; Taneda 1968; Eloy et al. 2012) showed that the film flutter is approximately periodic. And so is the jet flapping, because the latter is surely synchronized with the former. It follows that the power spectrum frequency (f) distribution (Φ_u), or simply called spectrum, of the fluctuating velocity (u) can be used to determine the flapping frequency (f_F). Figure 6 displays the spectra measured at $x/D = 3$ and $Re = 30,000$ for the jets from the three nozzles with a film (flapping) and without

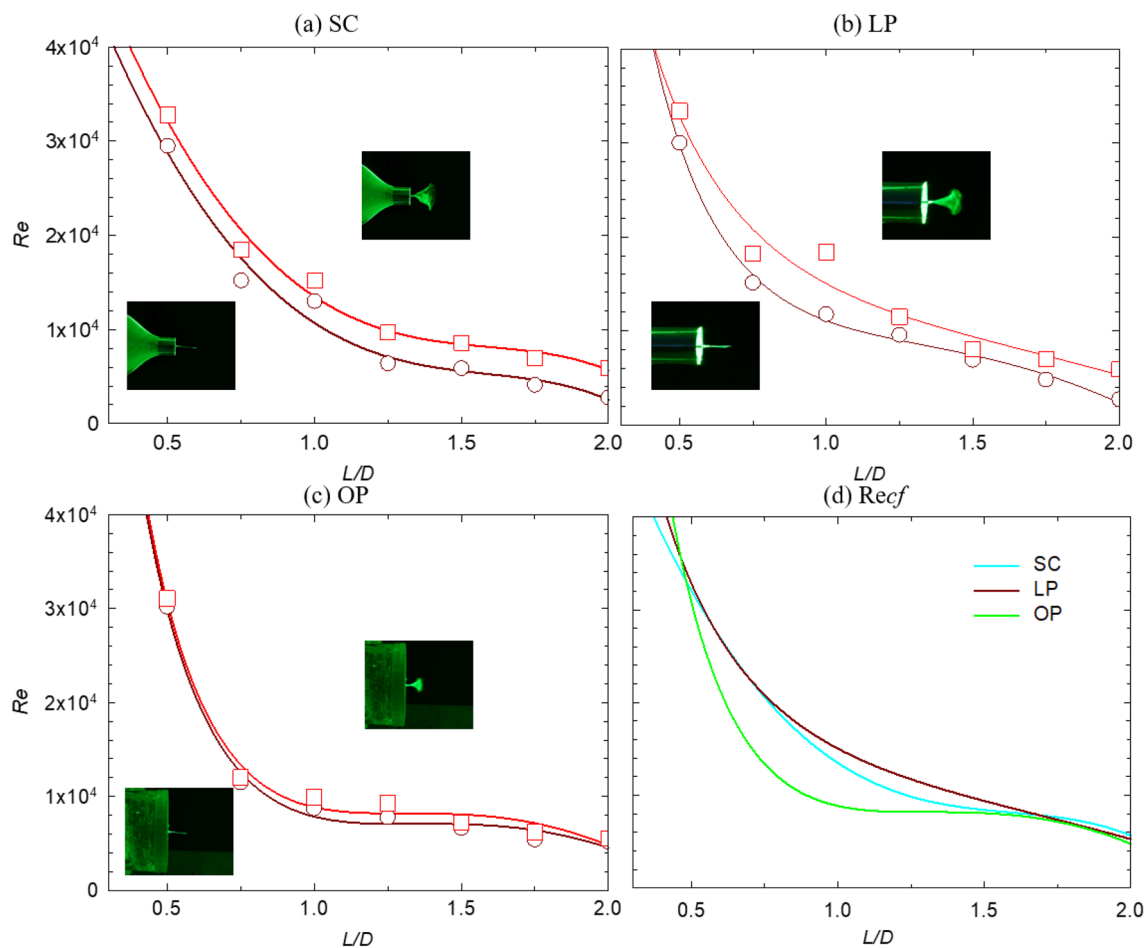


Fig. 4 Critical Reynolds numbers for the flutter of an FEP film to onset & rest (Re_{cf} & Re_{cr}) against L/D . **a** SC, **b** LP, **c** OP; and **d** comparison of Re_{cf} . Symbols: Re_{cf} ; Re_{cr}

film (non-flapping). At first, let us inspect the non-flapping or free jets. Evidently, a broad peak or hump occurs in Φ_u for either SC or OP jet but not for the LP jet. This peak is associated with the primary vortex structures formed by natural instability. The broad-peak frequency represents the averaged vortex passage frequency (f_p), whose dimensionless value or Strouhal number can be defined by $St_p \equiv f_p D / U_o$. The Strouhal numbers obtained at $x/D = 3$ and $Re = 30,000$ are approximately 0.61 and 0.7, respectively, for the free SC and OP jets, as indicated in Fig. 6a, c. Very differently, the broad peak does not appear in Φ_u for the free LP jet, suggesting few primary coherent structures to form that travel downstream quasi-periodically. The above observations are consistent with the findings of Mi et al. (2001c). These investigators comprehensively explained what is behind the observed distinctions, i.e., different underlying turbulence structures in the three jets. As shown in Fig. 2, the exit profile of the LP jet is of the power law of one-fifth in relation to a fully developed pipe flow, while that of the SC jet is nearly uniform and that of the OP jet is in the shape of M, i.e., the

mean velocity distributes axisymmetrically with its value at the center being U_{oc} and its maximum ($\approx 1.9U_{oc}$) locating at $r/D \approx 0.4$ near the nozzle edge. So, initially the OP and SC jets have very high velocity gradients with the surrounding fluid so as to form, by natural instability, large-scale coherent vortex structures in the axisymmetric and/or helical modes which are approximately periodically shedding and travel downstream. In contrast, the LP jet has a far smaller velocity gradient and a much higher turbulence intensity across the exit plane, which makes it difficult to sequentially form large-scale vortex structures with the ambient fluid. Even though there are some coherent structures, they must be shedding aperiodically and do not occur regularly.

Now we examine the flapping-jet spectra of Fig. 6. It is obvious that no broad peak similar to the free jet one occurs in Φ_u for any flapping jet, perhaps due to the global flapping motion suppressing the occurrence of natural instability. Instead, there are numerous sharp peaks or high spikes in Φ_u for all the OP, SC and LP jets. The first spike corresponds to the flapping frequency (f_p). It also can be seen that all the

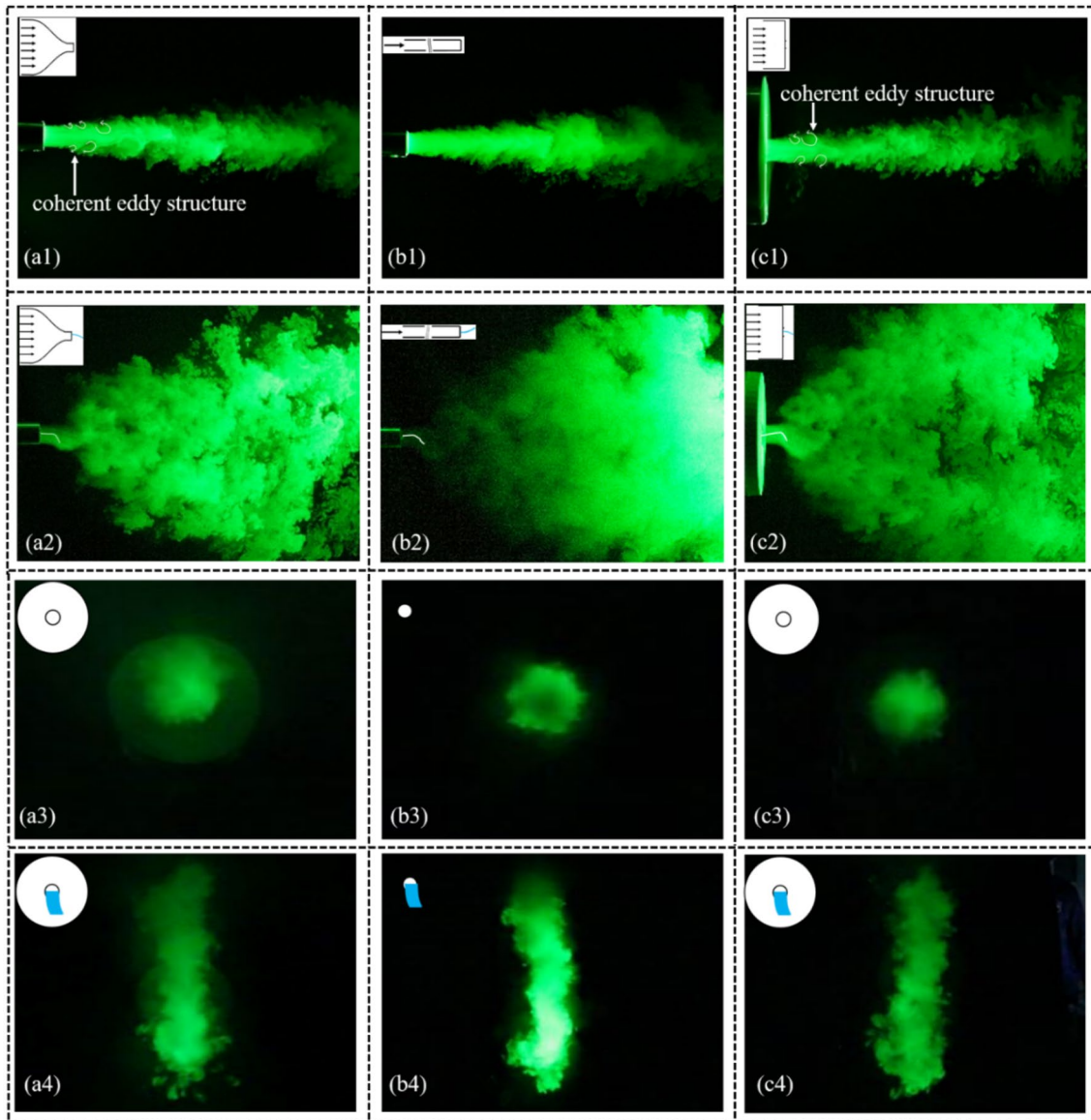


Fig. 5 Instantaneous images of the smoked free and flapping jets from **a** SC, **b** LP and **c** OP nozzles taken at $Re=30,000$. Free & flapping jets: (a1–c1) & (a2–c2) images through the central xy plane

approximately at $0 \leq x/D \leq 15$ and $-6 \leq y/D \leq +6$; (a3–c3) & (a4–c4) images through the yz plane at $x/D=5$ and $-6 \leq y/D \leq +6$

flapping jets have multiple frequency-multiplied peaks after the first one, indicating a good periodicity of the flapping. Moreover, Fig. 6 shows that f_F is significantly lower than the vortex passage frequencies ($St_p \approx 0.61$ and 0.7) for the free SC and OP jets.

Figure 7a demonstrates the dependence of f_F on the jet-exit Reynolds number (Re) for the three flapping jets. It can be seen that f_F increases linearly as Re rises. Specifically, the flapping frequency always maintains higher for the OP jet whereas it does not exhibit any significant difference for the LP and SC jets at all Re considered. These observations coincide with the film-flutter domain that is largest for the OP jet and nearly identical in the LP and SC cases,

see Fig. 4d. In addition, the increase in Reynolds number appears to weaken the influence of the exit conditions, so that the difference in f_F between the three jets becomes smaller.

Figure 7b shows the Re -dependent flapping Strouhal numbers defined by $St_F(D) \equiv f_F D/U_o$ and $St_F(A) \equiv f_F A/U_o$. Evidently, as Re grows from 20,000 to 45,000, $St_F(D)$ increase from 0.17 to 0.20 while $St_F(A)$ increases from about 0.14–0.20 for the flapping SC and LP jets. By comparison, for the flapping OP jet, since either A or f_F is greater, its two Strouhal numbers both stand on top at any Re , i.e., they are largest. It is also interesting that $St_F(A)$ is considerably greater for the OP jet (0.20–0.24) than for

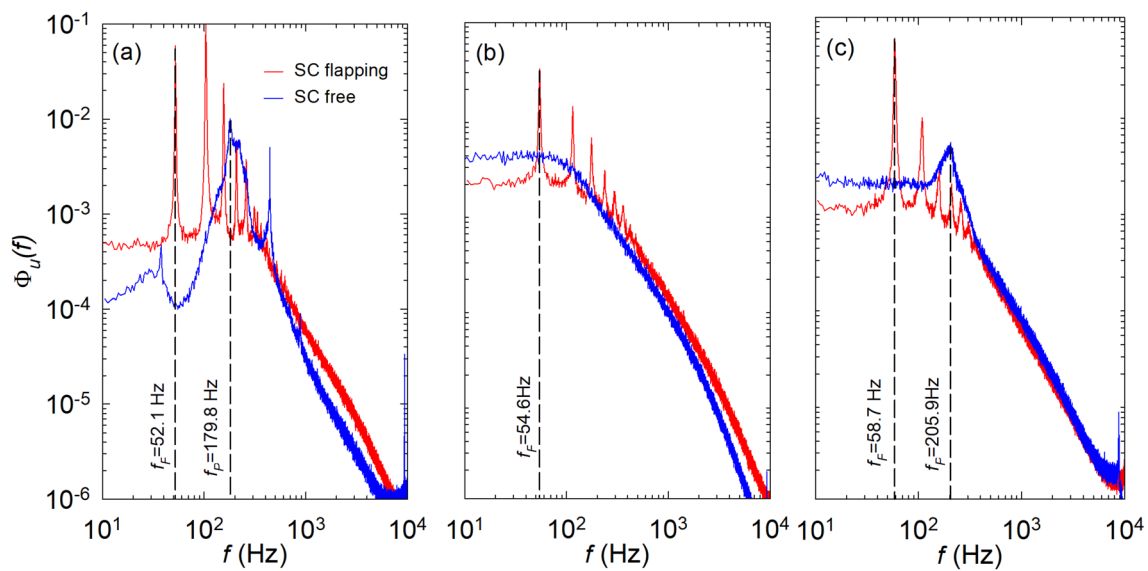


Fig. 6 Power spectra of the velocity fluctuations, Φ_u , obtained at $x/D=3$ in the shear-layers of axisymmetric jets issuing from **a** SC, **b** LP and **c** OP nozzles for $Re=30,000$

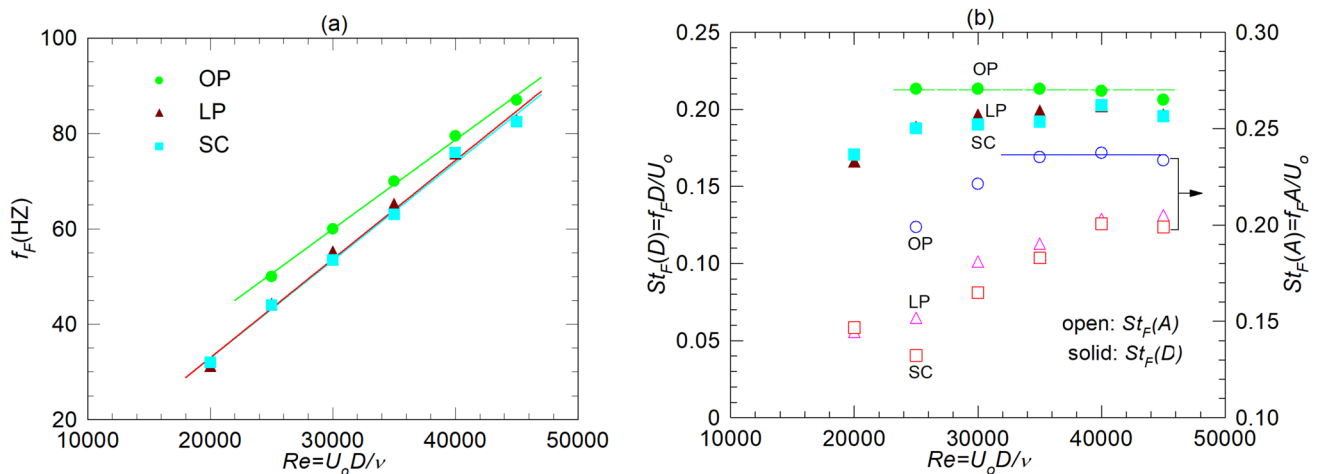


Fig. 7 **a** Jet-flapping frequency f_F and **b** Strouhal numbers $St_F(D)$ and $St_F(A)$ versus the Reynolds number Re for the flapping SC, LP and OP jets

the SC and LP jets (0.13 ~ 0.20). Moreover, $St_F(D)$ varies less than $St_F(A)$ with Re generally for the three jets. The reason for this is that D is a constant whereas A varies with Re (see Fig. 3b). In addition, both $St_F(D)$ and $St_F(A)$ of the three flapping jets are substantially lower than the natural vortex passage Strouhal number St_p for the free SC and OP jets. This suggests that the jet flapping is such a global motion whose scale is much (about 3×) greater than that for the primary coherent structure developing from the natural aerodynamic instability.

Next, the turbulent mixing characteristics of the three flapping jets will be investigated for $Re = 30,000$ with

different Strouhal numbers: $St_F(D) = 0.213$ (OP), 0.195 (LP) & 0.19 (SC) or $St_F(A) = 0.22$ (OP), 0.18 (LP) & 0.165 (SC). Of note, when $Re = 30,000$, the natural vortex passage Strouhal number $St_p \approx 0.61$ and 0.7, respectively, for the free SC and OP jets. Namely, St_p is around 15% higher for the OP jet than the SC free jet. Perhaps coherently, $St_F(A)$ of the flapping OP jet is about 22% and 33% higher than those of the SC and LP jets. These discrepancies will be reflected in distinct turbulent mixing characteristics shown below in Sects. 3.3 and 3.4.

3.4 Mixing characteristics of flapping jets versus free jets

3.4.1 Mean velocity and turbulence intensity

Figure 5 visually shows a huge difference in mixing characteristics between the smoked flapping and free jets. Laterally in the y direction, the flapping jets spread out far more widely and so occupy a much larger area than do the free jets. In other words, the former jets entrain and mix globally with much more ambient fluid. As a consequence, it is deduced qualitatively that, as the downstream distance x increases, the flapping jets should decay substantially faster, and hence their centerline mean velocity should decrease far more rapidly, than the free jets. Indeed, it is the case, as demonstrated in Fig. 8a, which shows the centerline U_{oc}/U_c for all the six jets at $Re = 30,000$. Here, U_c and U_{oc} are the centerline mean velocity and its exit value. Moreover, Fig. 8b displays the centerline turbulence intensity u_c'/U_c where $u_c' = \langle u_c'^2 \rangle^{1/2}$. For comparison, the free SC jet results of Mi and Nathan (2010) for $Re = 15,000$ are also presented in Fig. 8a, b. Giving different Reynolds numbers and other uncertain conditions, we consider a reasonable consistency of the present results with those of Mi and Nathan (2010), indirectly validating our hot-wire measurements.

Careful inspection finds that, for the free jets, U_c exhibits a roughly-constant portion over a short distance immediately downstream from the nozzle exit (i.e., at $x/D \leq 5$), which corresponds to the traditionally so-called ‘potential core’ where the ‘unmixed’ fluid maintains uniformly at the same velocity on average. The flapping jets

do not have this portion due to the whole-jet oscillation. As the flow proceeds farther downstream, Fig. 8a, all the jets exhibit an approximately linear variation of U_{oc}/U_c against the downstream distance x for $x/D \geq 6-10$; i.e., $U_{oc}/U_c \propto K(x/D)$, where the slope K represents the decay rate of U_c . A few observations can be made from the plot. First, the flapping jets decay at much higher rates than do the free jets. As a result, the slope K for the former (0.32–0.48) is far greater than that (0.12–0.18) for the latter. That is, relative to the non-flapping free jets, all the present flapping jets entrain and mix the surrounding fluid at a much higher rate. Second, close values of K or compatible variations of U_{oc}/U_c are observed in the SC and LP jets, either free or flapping, versus a substantially higher slope K in the OP case. In other words, when the SC and LP jets develop downstream quite similarly, the OP jets decay and spread out much more rapidly, no matter whether the jets are flapping or not. This is consistent with the scalar measurements of Mi and Nathan (2010).

Consistent with the jet-dependent differences in U_{oc}/U_c revealed above, Fig. 8b demonstrates significant discrepancies in u_c'/U_c or the turbulence intensity between the six jets. Very obviously, the magnitude of u_c'/U_c is far higher in the flapping jets than that in the free jets. Especially, the turbulence intensity exhibits a hump over $2 < x/D < 7$ in the flapping jets versus its gradual growth in the free SC and LP jets. It is interesting that u_c'/U_c shows a broader hump in the free OP jet. As x grows further, u_c'/U_c slowly varies and appears to approach asymptotically to a constant at $x/D > 15-20$. However, in the far-field flapping jets ($x/D > 20$), u_c'/U_c remains significantly higher than in the free jets. In the whole measured flow field, the turbulence intensity maintains to be highest in the flapping OP jet and

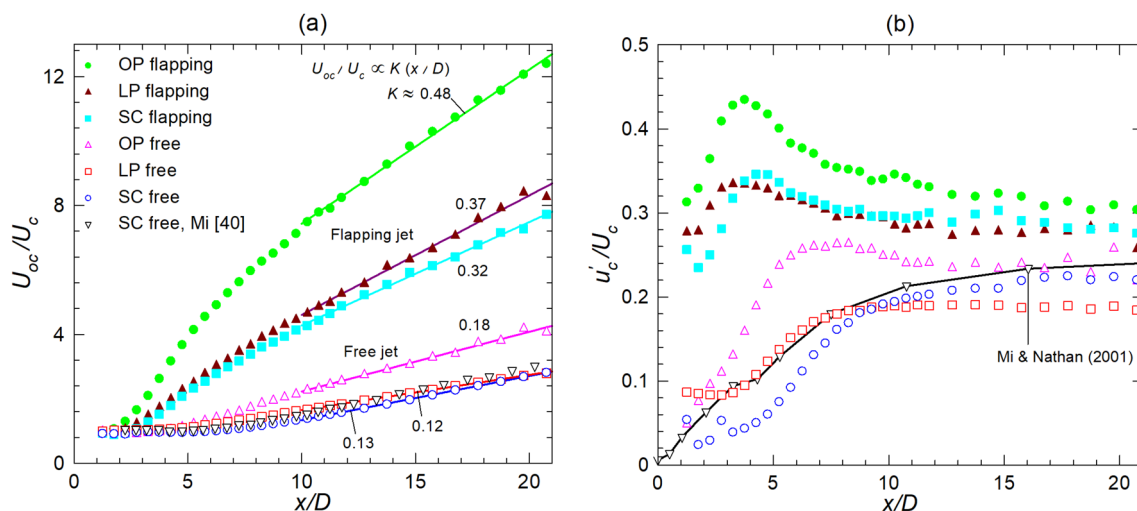


Fig. 8 **a** Inverse ratio (U_{oc}/U_c) of the centerline mean velocity (U_c) to its exit value (U_{oc}) and **b** the turbulence intensity (u_c'/U_c) for all jets of investigation at $Re = 30,000$

compatible in the flapping SC and LP jets. These findings appear to agree very well with the results of Fig. 7 for the jet-flapping frequency and Strouhal numbers. For instance, $St_F(A)$ of the flapping OP jet is about 22% and 33% higher than those of the SC and LP jets for $Re = 30,000$. In this context, it is deduced that the higher the flapping Strouhal number, the stronger the large-scale mixing. Relative to the conventional (non-flapping) free jets, all the present flapping jets entrain and mix the surrounding fluid at a much higher rate, consequently spreading and decaying far more rapidly.

3.4.2 Probability density function (PDF) of the velocity fluctuation

Both the mean velocity and turbulence intensity distributions of Fig. 8 partially characterize the global mixing of each jet or display large-scale mixing characteristics of the jets. However, these two parameters ($U_{oc}/U_c, u_c'/U_c$) cannot reflect the truly detailed mixing at different scales, especially at the smallest level or the mixedness between the ejecting and surrounding fluids. To assess how deep the turbulence mixing takes place at the finest scales in these turbulent jets, the probability density function (PDF) of $u_c(t)$, denoted by $P(u_c)$, should be examined, even though it is also not perfect for assessing the turbulent mixing. Ideally, in homogenous turbulent flows (where the mean shear rate or mean velocity

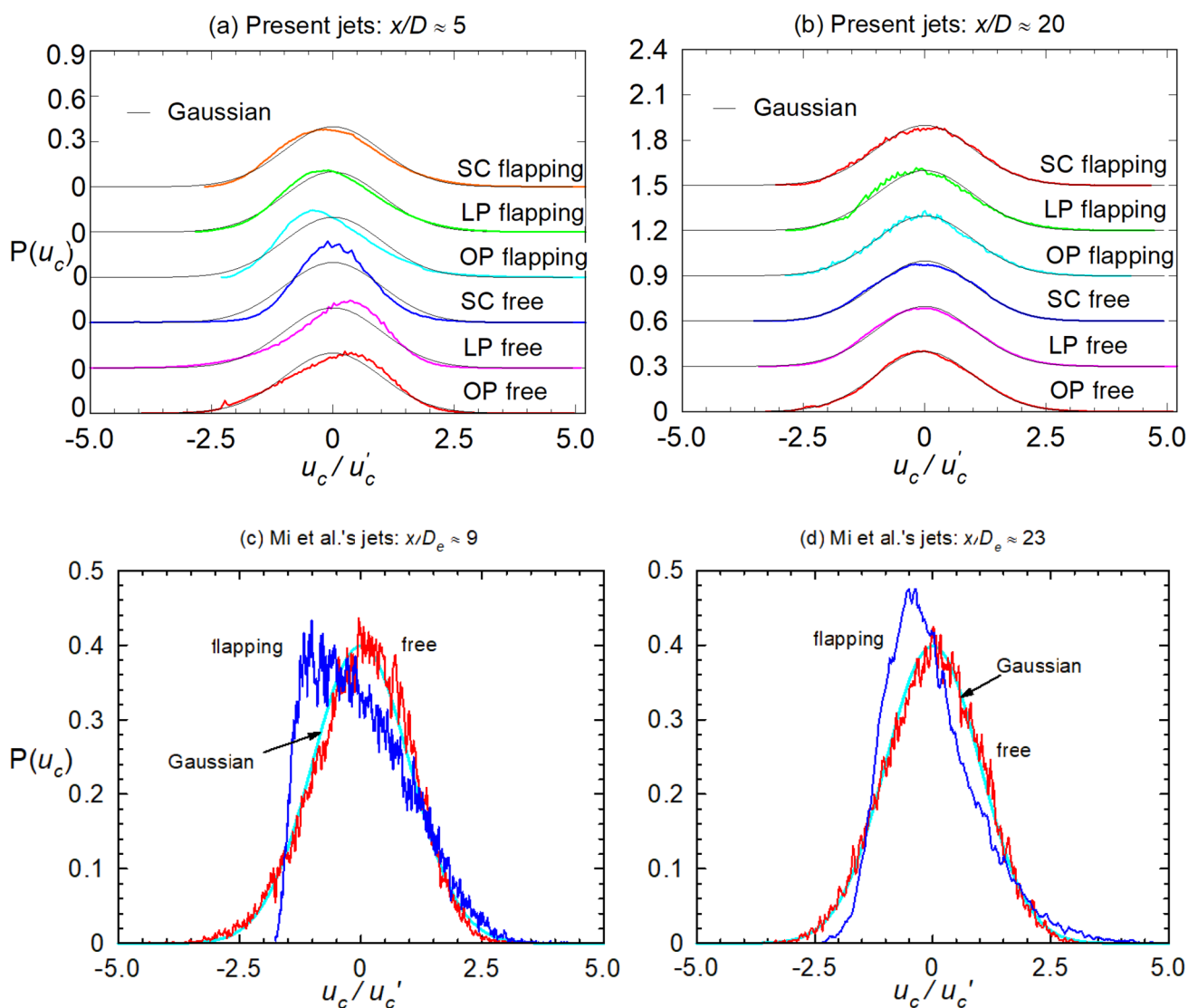


Fig. 9 Probability density function of the centerline fluctuating velocity, $P(u_c)$. Present circular jets for $Re = 30,000$: **a** $x/D \approx 5$ and **b** $x/D \approx 20$; Mi et al. (2001a)'s rectangular jets for $Re = 15,500$: **c** $x/D_e \approx 9$ and **d** $x/D_e \approx 23$

gradient is zero), the more closely the distribution of $P(u_c)$ is Gaussian, the more deeply and thoroughly the smallest-scale turbulent mixing is expected to occur; the Gaussianity of $P(u_c)$ represents the thorough mixing in this special case.

Figure 9a, b shows the centerline $P(u_c)$ distributions versus the Gaussian for all the present jets obtained at $x/D \approx 5$ and 20. It is demonstrated that, at $x/D \approx 5$, $P(u_c)$ differs from the Gaussianity for all the jets; such a difference seems greater in the free jets than the flapping ones.

Specifically, $P(u_c)$ takes the maximum distinctly on the negative or positive sides of u_c for the flapping or free jets. This indicates that, at $x/D \approx 5$, the ejecting fluid occupies the centerline for a longer time than the entrained ambient fluid for the free jets, versus the opposite for the flapping jets. Because the streamwise velocity of the ambient fluid is much lower than that of the ejecting fluid, the free jets show a positive skewness in their PDFs while the flapping jets exhibit a negative skewness. Moreover, Fig. 9a

Fig. 10 Normalized distributions of the frequency spectrum (Φ_u) of the centerline $u_c(t)$ of the flapping and free jets at $Re = 30,000$: **a** $x/D \approx 5$ and **b** $x/D \approx 20$

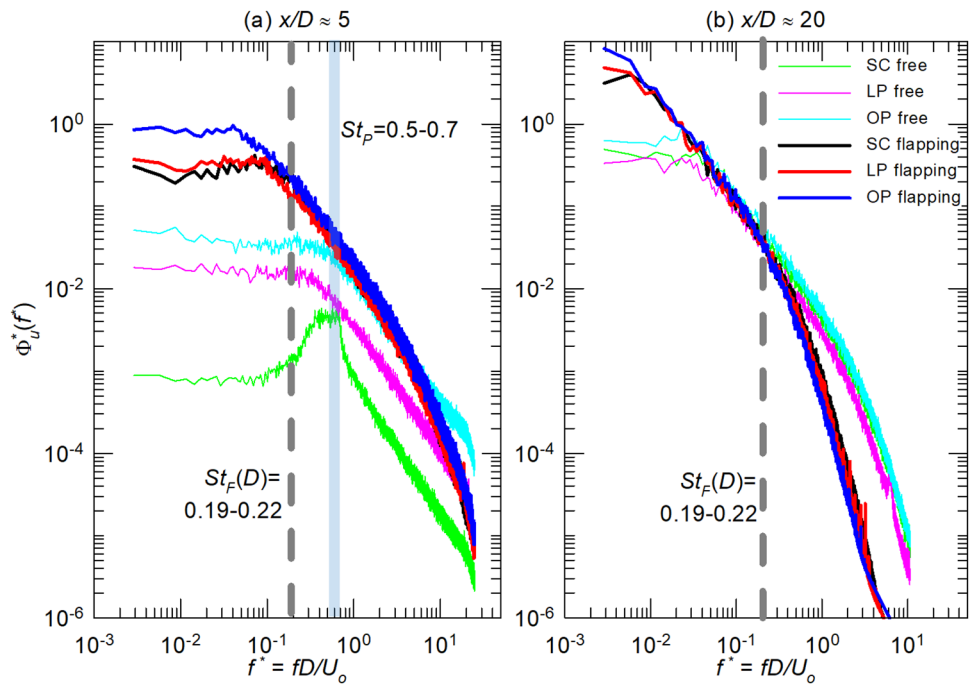
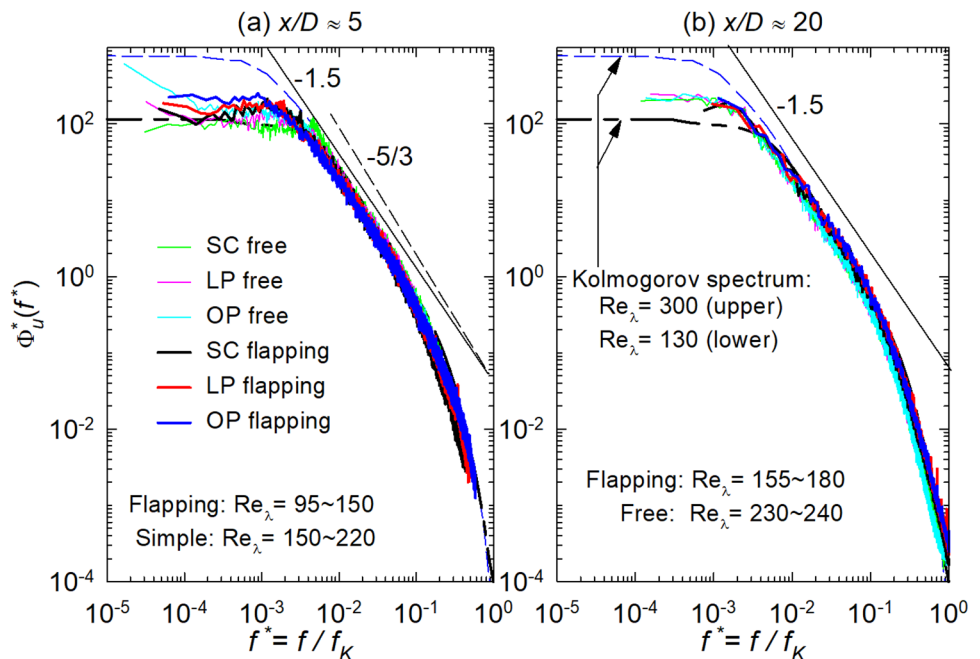


Fig. 11 Normalized power spectrum (Φ_u) of the centerline $u_c(t)$ of the flapping and free jets at $Re = 30,000$: **a** $x/D \approx 5$ and **b** $x/D \approx 20$. The normalization is taken so that $\int_0^\infty \Phi_u^* df^* = 1$ and $f^* = f/f_K$, where $f_K = U_c/(2\pi\eta)$



illustrates that $P(u_c)$ is closer to the Gaussian distribution in the flapping jets than in the free jets. This observation leads to a postulation that the reeling in of the surrounding fluid by the fast flapping motion may facilitate the occurrence of better small-scale mixing all the way from the near-nozzle region to the far field. Further, it can be seen from Fig. 9a that the near-field PDF deviates more from Gaussian for the flapping OP jet than for the other flapping jets. This is because the flapping OP jet is most deflected, so having the strongest large-scale mixing ability on the surrounding fluid but delayed fine-scale mixing. At $x/D \approx 20$ in both the free and flapping jets (Fig. 9b), $P(u_c)$ distributes nearly Gaussian, indicating a thoroughly fine-scale mixing on the centerline in all the present jets.

The above observations appear to differ from those made by Mi et al. (2001a) based on their comparisons of the fluidic flapping jet from a rectangular slot nozzle (whose width and height are $w=8.5$ mm and $h=0.6$ mm) with the free counterpart, both at $Re=15,500$. They compared their PDFs of u_c in their Fig. 15, which is presently reproduced in Fig. 9c, d. Their axial and lateral components (u, v) of the fluctuating velocity measured at $x/D_e \approx 9$ and 23 or $x/h \approx 37.5$ and 96 ; here D_e is the equivalent diameter (≈ 2.5 mm) of a circular exit with the same area of the rectangular slot. Based on the slot exit conditions and the flapping frequency $f_F=100$ Hz, the flapping jet of Mi et al. (2001a) operated at the Strouhal number of $St_F(D_e) \approx 2.8 \times 10^{-3}$ or $St_F(h) \approx 6.7 \times 10^{-4}$. Obviously, their flapping Strouhal number is much smaller than those of the present jets ($St_F(D) \approx 0.19-0.22$). Mi et al. (2001a) claimed that, relative to the non-flapping one, their flapping jet enhances the large-scale entrainment and suppresses the fine-scale turbulent mixing simultaneously. Indeed, Fig. 9c, d demonstrates a higher probability of the occurrence of the lowest velocity fluid in their flapping jet than in their free jet, as indicated by the sharp cut-off and steep drop in $P(u_c)$ on the negative u_c side, respectively, for $x/D_e=9$ and 23 . This indicates a significant increase in the quantity of low- U fluid across the centerline of the flapping jet all the way from the near to far field. That is, the bias in $P(u_c)$ with low velocities should arise from occasional appearance of the entrained, yet poorly mixed or even unmixed, fluid parcels brought by the upstream flapping motion. By contrast, their free rectangular jet was much better mixed with the surrounding fluid, particularly at the finest scales in the central region where $P(u_c)$ is nearly Gaussian at $x/D_e \geq 9$.

3.4.3 Power spectrum of the fluctuating velocity

Figure 10 compares the normalized power spectra of u_c for the flapping jets with those for the free jets; the presentation is in the log-log form to see clearly the low-frequency portion for the large-scale contribution. The normalization

taken for the plots is such that $\int_0^\infty \Phi_u^* df^* = (u'_c/U_o)^2$ where $f^* = fD/U_o$. As a reference, the Strouhal numbers of the jet-flapping ($St_F(D)$) and natural vortex passage ($St_P(D)$) are indicated by vertical lines on the plots. Figure 9a demonstrates that the u_c -spectra are much greater over the whole frequency range for the present flapping jets than those for the free jets in the near field at $x/D=5$. This appears to imply that the flapping motion greatly enhances the near-field jet's turbulent fluctuations over all flow scales, including the smallest-scale fluctuation, which perhaps boosts the fine-scale or even molecular-level mixing between the nozzle-ejecting and ambient fluids. Because the fine-scale mixing is enhanced, the centerline velocity PDFs of the flapping LP and SC jets exhibit a closely Gaussian distribution at $x/D=5$ (see Fig. 9a). This enhancement should maintain farther downstream into the far field, so that $P(u_c)$ is nearly Gaussian at $x/D=20$, even though $\Phi_u(f^*)$ at $f^* \geq 0.4$ for the flapping jets drops below that of the free jets, see Fig. 9b.

It is also worthy to note that, at $f^* = fD/U_o < 0.06$, the near-field spectrum Φ_u^* in the OP flapping jet is about 200% greater than that in the other two flapping jets. This indicates that the large-scale fluctuation in u_c in the OP flapping jet is much stronger. Even farther downstream at $x/D=20$, Φ_u^* maintains substantially higher at $f^* = fD/U_o < 0.006$ in the OP flapping jet. Nevertheless, for $f^* > 0.06$ at $x/D=5$ or $f^* > 0.006$ at $x/D=20$, Φ_u^* is nearly identical, demonstrating statistically indistinguishable mixing motions at intermediate and small scales, for all the three flapping jets. These observations are consistent with those made from Figs. 8 and 9, which all point to the strongest large-scale mixing of the OP flapping jet.

To inspect the small-scale mixing, Fig. 11 displays the spectra of $u_c(t)$ normalized by the Kolmogorov frequency $f_K = U_o/(2\pi\eta)$, where η is the Kolmogorov length scale (see Sect. 3.4 for its definition). Since f_K represents the average frequency of the smallest-scale fluctuations of $u_c(t)$, the f_K -normalized power spectrum should far more appropriately reflect the real turbulent mixing at the smallest scales than those of Fig. 10 (normalized by U_o and D). Strikingly, the normalized spectra of all the jets well collapse over quite a wide range of f , i.e., nearly the entire f range for $x/D \approx 20$ and at $f/f_K > 0.003$ for $x/D \approx 5$. In particular, there is a power-law region occurring in the spectrum over a certain range of f , i.e., $\Phi_u \propto f^{-m}$ where $m \approx 1.5$ (as indicated on the plots), for both the free and flapping jets. Note that the value of $m \approx 1.5$ was also obtained on the jet centerline by several previous studies of a free circular jet for widely different Reynolds numbers (Mi and Antonia 2001; Mi et al. 2013; Burattini et al. 2005). Interestingly, this power-law exponent is not the famous Kolmogorov exponent of $5/3$. It is worth noting that, according to Mi and Antonia (2001), the appearance of a power-law range should signify the presence of the

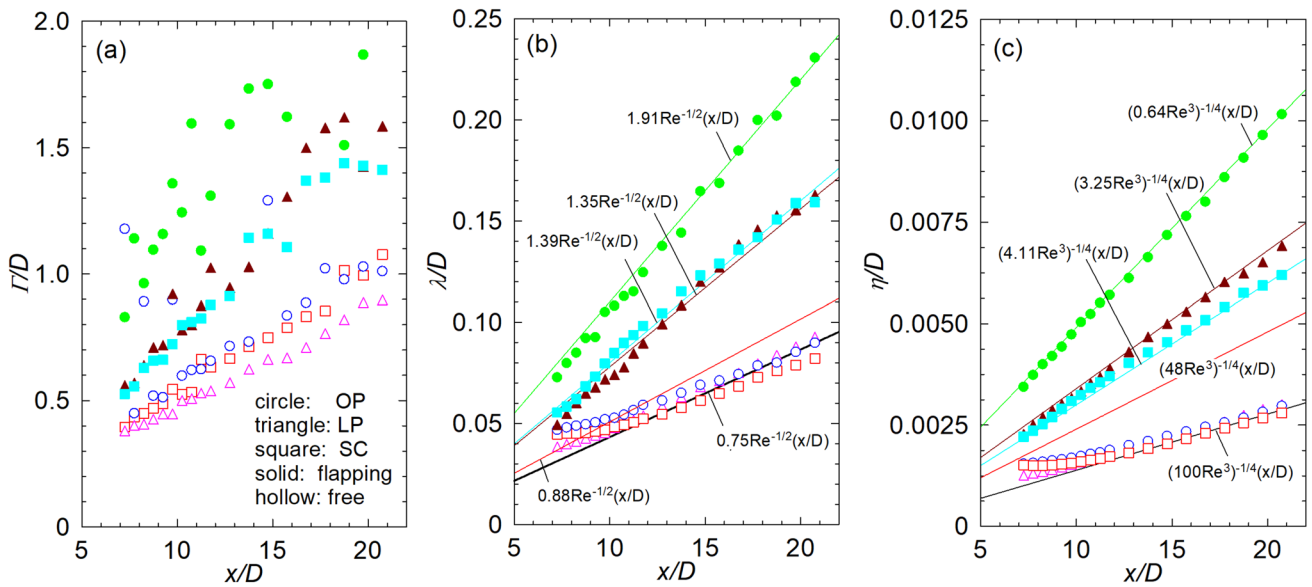


Fig. 12 Centerline turbulence length scales of the flapping jets at $Re=30,000$ from different (SC, LP & OP) nozzles: **a** integral scale (Γ); **b** Taylor microscale (λ); and **c** Kolmogorov length (η)

inertial range of turbulence, through which energy transfers down independently of viscosity from large to small scales. As a reference, the normalized model Kolmogorov spectra for $Re_\lambda = 130$ and 300 are also displayed; relatively, the present values of Re_λ for both the flapping and free jets are indicated on the plots. It is indeed surprised that the present spectra agree perfectly with the Kolmogorov spectrum at $f/f_K > 0.003$ for $Re_\lambda = 130$.

The above observations from Fig. 11 may suggest that, on the centerline at $x/D \geq 5$, the truly turbulent mixing in the flapping jets becomes similar to that in the free jets. This is consistent with the implication of $P(u_c)$ that is nearly Gaussian for both the free and flapping jets. This also contrasts with the fluidic low-Strouhal-number flapping jet of Mi et al. (2001a) where the centerline $P(u_c)$ is highly non-Gaussian all the way from the near field to the far field (Fig. 9c, d).

3.5 Characteristic scales of turbulent mixing of flapping jets versus free jets

Traditionally, large, intermediate and small-scale turbulence structures can be characterized, respectively, by the integral (Γ), Taylor (λ), and Kolmogorov (η) length scales obtained from the instantaneous signal of the streamwise velocity $u(t)$. The integral length is usually estimated by

$$\Gamma = U_{con} \int_0^{\tau_0} \langle u(t)u(t + \tau) \rangle \langle u^2 \rangle^{-1} d\tau \tag{1}$$

where U_{con} is the averaged convection velocity and τ_0 corresponds to the first zero crossing of the autocorrelation

function $\langle u(t)u(t + \tau) \rangle$. The Taylor length scale is obtained by

$$\lambda = \langle u^2 \rangle^{1/2} / \langle (\partial u / \partial x)^2 \rangle^{1/2} \tag{2}$$

while estimating the Kolmogorov length scale via

$$\eta = (\nu^3 / \epsilon)^{1/4} \tag{3}$$

Here, ϵ represents the mean turbulence energy dissipation rate obtained by assuming the locally isotropic turbulence so that $\epsilon = 15\nu \langle (\partial u / \partial x)^2 \rangle$; note that $\partial u / \partial x = (U_c)^{-1} \partial u / \partial t$ is based on Taylor's hypothesis.

Friehe et al. (1972) obtained the following empirical relations of λ and η versus x for a free circular SC jet in the self-preserving region

$$\lambda/D = aRe^{-1/2}(x/D) \tag{4}$$

and

$$\eta/D = (bRe^3)^{-1/4}(x/D) \tag{5}$$

with $a=0.88$ and $b=48$. In general, the parameters a and b are experimental constants depending upon the jet's initial conditions. Later, Antonia et al. (1980) validated Eqs. (4) and (5), identically with $a=0.88$ and $b=48$, in several free circular jets. Interestingly, Eqs. (4) and (5) also work for non-circular free jets (Mi and Nathan 2010) and even flapping jets (Wu et al. 2020) when modifying a and b from 0.88 and 48.

Figure 12a–c shows the centerline variations of the three length scales (Γ , λ and η) for all the present free and flapping SC, LP and OP jets. At the first glance, it is straightforward to observe that all the three length scales on centerline increase approximately linearly with the downstream distance x generally for all the jets, no matter whether they are flapping or not. Another observation can be made that these scales are far greater in the flapping jets than in the free jets. This implies that the flapping motion enlarges all the turbulence scales. Moreover, while the centerline λ and η are not much different for the three free jets, they are far larger for the flapping OP jet than for the flapping SC and LP jets. Notably, in the flapping SC and LP jets, both Γ and λ are compatible while η is greater at $x/D > 12$ in the latter. In addition, it is worth noting from Fig. 12a that a highly scattering occurs in the integral-scale data. The large scatter for the flapping jets may be caused by both the estimate method associated with Eq. (1) and the flapping motion. However, not only the scatters of λ and η are much smaller but also the linearities of λ and η versus x are much better than that of Γ . These discrepancies may be attributed to the different effects of the flow inlet conditions on different scales of turbulence. It is anticipated that the large-scale turbulence properties should be more sensitive to changes of the inlet and boundary conditions than the small-scale ones.

At last, worth noting is that both Eqs. (4) and (5) work well for either the free jets or the flapping jets, as unmistakably demonstrated by Fig. 12b, c. The two relationships are validated with $a \approx (1.91, 1.39, 1.35)$ and $b \approx (0.64, 4.11, 3.25)$, respectively, for the flapping OP, SC and LP jets at $x/D \geq 7$. In contrast, Eqs. (4) and (5) with $a \approx 0.75$ and $b \approx 100$ appear to work for all the free jets at $x/D \geq 12$. This has further confirmed the universality of the relationships (4) and (5). Nevertheless, unlike the flapping jets, the free jets exhibit their data of λ and η that would not follow Eqs. (4) and (5) at $x/D < 12$. This discrepancy does not represent the real case but reflects the error caused certainly by the poor resolution of the fixed sampling frequency ($= 50,000$ Hz). This frequency is too slow and cannot fully resolve λ and η , whose true values are very small, in the near-field region of the free jets. As seen clearly in Fig. 12b, c, λ and η are far greater in the flapping jets than in the free jets. Thus, when sampling the velocity signal at the same frequency for all the jets, the temporal resolution of $u(t)$ is relatively poorer for the free jets. So, in the free jets at $x/D < 12$, both λ and η are overestimated because $\langle (\partial u / \partial x)^2 \rangle$ is underestimated (see Eqs. (2) and (3)).

3.6 On the nature-vortex shedding and jet-flapping Strouhal numbers

As reflected in the exit distributions of the mean and RMS velocities, Fig. 2, the SC, LP and OP nozzles form dissimilar

initial flow conditions for the jets issuing downstream. Besides, the near-field flow structures are also distinct in the three jets. In particular, very different from the SC and LP cases, the OP jet often shows a short ‘vena contracta’ whose minimum cross section is at least 30% smaller than that of the nozzle exit (see Mi et al. 2001c). So, the present OP jet is anticipated to be either more ‘flexible’ for film-induced flapping or with a higher velocity to roll up primary vortices by natural instability. Indeed, Fig. 6a, c demonstrates through the u spectra that the free OP jet’s primary vortex structures travel downstream generally at a higher passage frequency (f_p) or Strouhal number (St_p) than that for the free SC jet; e.g., when $x/D = 3$ and $Re = 30,000$, $f_p \approx 206$ Hz and $St_p \approx 0.7$ for the former versus $f_p \approx 180$ Hz and $St_p \approx 0.61$ for the latter. That is, St_p for the OP jet is 14.8% higher than that for the SC jet. (Unfortunately, f_p and St_p cannot be obtained from the near-field u spectrum of the free LP jet, because few or no primary structures are formed periodically in this jet.) Likewise, similar differences occur between the flapping OP, SC and LP jets: i.e., the flapping frequency f_f and Strouhal number St_f with the OP case are considerably higher than those with the SC and LP cases for all the tested Reynolds numbers (see Fig. 7). For example, at $Re = 30,000$, $St_f(A) = 0.22$ (OP), 0.18 (LP) & 0.165 (SC); namely, $St_f(A)$ of the flapping OP jet is about 22% and 33% higher than those of the SC and LP jets.

With the highest St_p , the free OP jet develops downstream at the highest velocity decay rate and strongest relative turbulence intensity, among the free jets. Similarly, with the highest St_f , the flapping OP jet operates at the highest velocity decay rate, strongest relative turbulence intensity, and also largest values of various turbulent length scales; on the other hand, the flapping SC and LP jets are generally compatible in mixing characteristics. In other words, the flapping OP jet exhibits substantially distinct mixing characteristics from those of the SC and LP jets. This suggests that $St_f(A)$ is more appropriate than $St_f(D)$ to act as the Strouhal number for research into the flapping jets, since the difference in St_f between the flapping OP jet and the other two is greater when using A rather than D as the length scale.

According to the results of Sect. 3.5, when the flapping Strouhal number is sufficiently high or low, the corresponding flapping motion appears to enhance or depress the small-scale turbulence mixing in the near field and then maintain farther downstream. It is postulated that St_f should have critical values for the enhancement and depression, which are currently unknown. Nevertheless, the present authors would like to address this issue by undertaking more experiments in near future.

4 Conclusion

The present study has experimentally examined particular effects of initial flow conditions on the turbulent mixing characteristics of a flapping jet versus its free counterpart; each flapping jet was ‘self-excited’ by a FEP film with one end fixed at the nozzle exit. The distinct initial conditions were made through three nozzles of different geometric configurations of smooth contraction (SC), long pipe (LP), and orifice plate (OP). Based on the results of Sect. 3, we can conclude that, overall, the characteristics of both film flutter and jet mixing depend greatly on the inflow condition. More specifically, it is concluded from the present work that:

- (1) The OP nozzle yields the largest flutter domain, highest flutter frequency and lowest energy loss for film flutter to occur;
- (2) The flapping OP jet is characterized by the highest flapping Strouhal number, highest velocity decay rate, strongest relative turbulence intensity, and largest values of various turbulent length scales, while the flapping SC and LP jets are overall compatible in mixing characteristics;
- (3) Relative to the conventional (non-flapping) free jets, all the present flapping jets entrain and mix the surrounding fluid at a much higher rate, consequently spreading and decaying far more rapidly.
- (4) When the flapping Strouhal number (St_F) is sufficiently high or low, the corresponding flapping motion appears to enhance or depress the small-scale turbulence mixing in the near field and then maintain farther downstream. It is postulated that St_F should have critical values for the enhancement and depression. This postulation is worthy to be confirmed by an experimental study in near future.

Acknowledgements The financial support of National Nature Science Foundation of China (Grant No. 11972048) is gratefully acknowledged.

References

Antonia RA, Satyaprakash BR, Hussain AKMF (1980) Measurements of dissipation rate and some other characteristics of turbulent plane and circular jets. *Phys Fluids* 23:695–700

Burattini P, Lavoie P, Antonia RA (2005) On the normalized turbulent energy dissipation rate. *Phys Fluids* 17:098103

Crow SC, Champagne FH (1971) Orderly structure in jet turbulence. *J Fluid Mech* 48:547–591

Danaila I, Boersma BJ (2000) Direct numerical simulation of bifurcating jets. *Phys Fluids* 12:1255–1257

Davis MR (1982) Variable control of jet decay. *AIAA J* 20:606–609

Eloy C, Kofman N, Schouveiler L (2012) The origin of hysteresis in the flag instability. *J Fluid Mech* 691:583–593

Favre-Marinet M, Binder G, Hac TV (1981) Generation of oscillating jets. *J Fluids Eng* 103:609–613

Friehe CA, Van Atta CW, Gibson CH (1972) Jet turbulence: dissipation rate measurements and correlations. In: *Turbulent shear flows, AGARD conference proceedings no. 93*, 18–1

Glauser M, Walker S (1988) Active flow control to cut millions from jet engine life cycle costs. *Air Force Res Lab Res Highlights*, Sept/Oct 1998

Gohil TB, Saha AK, Muralidhar K (2015) Simulation of the blooming phenomenon in forced circular jets. *J Fluid Mech* 783:567–604

Hill WG, Greene PR (1977) Increased turbulent jet mixing rates obtained by self-excited acoustic oscillations. *ASME J Fluids Eng* 99:520–525

Manias CG, Nathan GJ (1993) The precessing jet gas burner a low NO_x burner providing process efficiency and product quality improvements. *World Cement* (march) 1993:4–11

Mi J, Antonia RA (2001) Effect of large-scale intermittency and mean shear on scaling-range exponents in a turbulent jet. *Phys Rev E* 64:026302

Mi J, Nathan GJ (2010) Statistical properties of turbulent free jets issuing from nine differently-shaped nozzles. *Flow Turbul Combust* 84:583–606

Mi J, Nathan GJ, Luxton RE (2001a) Mixing characteristics of a flapping jet from a self-exciting nozzle. *Flow Turbul Combust* 67:1–23

Mi J, Nobes DS, Nathan GJ (2001b) Influence of exit conditions of round nozzles on the passive scalar field of a free jet. *J Fluid Mech* 432:91–125

Mi J, Nobes DS, Nathan GJ (2001c) Mixing characteristics of axisymmetric free jets issuing from a contoured nozzle, an orifice plate and a pipe. *ASME J Fluids Eng* 123:878–883

Mi J, Xu M, Zhou T (2013) Reynolds number influence on statistical behaviors of turbulence in a circular free jet. *Phys Fluids* 25:075101

Mi J, Nathan GJ, Luxton RE (2004) Oscillating jets, PCT/AU98/00959, US patent no. 6685102 (2004.2), European pat. no. 1032789 (2004.9)

Nathan GJ, Hill SJ, Luxton RE (1998) An axisymmetric ‘fluidic’ nozzle to generate jet precession. *J Fluid Mech* 370:347–380

Nathan GJ, Luxton RE (1991) Flame stability and emission characteristics of the enhanced mixing burner. The 2nd European conference on industrial furnaces and boilers, april. Portugal, Algarve

Païdoussis MP (2016) *Fluid-structure interactions: slender structures and axial flow*, vol 2. Elsevier, London

Parekh D, Leonard A, Reynolds WC (1983) A vortex-filament simulation of a bifurcating jet. *Bull Am Phys Soc* 28:1353

Raman G, Cornelius D (1995) Jet mixing control using excitation from miniature oscillating jets. *AIAA J* 33:365–368

Reynolds WC, Parekh DE, Juvet PJD, Lee MJD (2003) Bifurcating and blooming jets. *Annu Rev Fluid Mech* 35:295–315

Silva CBD, Métais O (2002) Vortex control of bifurcating jets: a numerical study. *Phys Fluids* 14:3798–3819

Simmons JM, Lai JCS, Platzer MF (1981) Jet excitation by an oscillating vane. *AIAA J* 19:673–676

Taneda S (1968) Waving motions of flags. *J Phys Soc Jpn* 24:392–401

Tyliszczak A (2015) LES-CMC of excited hydrogen jet. *Combust Flame* 162:3864–3883

Tyliszczak A, Geurts BJ (2014) Parametric analysis of excited round jets—numerical study. *Flow Turbul Combust* 93:221–247

Viets H (1975) Flip-flop jet nozzle. *AIAA J* 13:1375–1379

Wu M, Xu M, Mi J, Deo RC (2020) Mixing characteristics of a film-exciting flapping jet. *Int J Heat Fluid Flow* 82:108532

Xu M, Wu M, Mi J (2019) A new type of self-excited flapping jets due to a flexible film at the nozzle exit. *Exp Therm Fluid Sci* 106:226–233